DERIVING FIRST FLOOR ELEVATIONS (FFEs) WITHIN RESIDENTIAL COMMUNITIES LOCATED IN GALVESTON USING RTK-UAS BASED DATA

A Thesis

by

Nicholas David Diaz

Submitted to the Office of Graduate and Professional Studies of
Texas A&M University
in partial fulfillment of the requirements for the degree of

MASTER OF MARINE RESOURCE MANAGEMENT

Chair of Committee,	Wesley E. Highfield
Committee Co-Chair,	Samuel D. Brody
Committee Member(s),	Brent Fortenberry
Department Head,	Kyeong Park

August 2020

Major Subject: Marine Resource Management

ABSTRACT

Flood damages occur when just one inch of water enters a residential household and models of flood damage estimation are sensitive to first floor elevation (FFE). The current sources for FFEs consist of costly survey-based elevation certificates or assumptions based on the year built and foundation type. We sought to address these limitations by establishing the role of an RTK enabled UAS platform in deriving FFEs. Four residential communities within Galveston Island were chosen based on location, elevation differences, and structure types. A Phantom 4 RTK was used to obtain georeferenced aerial imagery of these communities to create detailed 3D models within Pix4D with +/- 0.02 m horizontal and +/- 0.035 m vertical accuracies. From these residential community models, ground, FFEs, and nearest drainage road elevations were obtained. Our findings, show that the RTK enabled UAS approach is an efficient, cost-effective method in establishing accurate FFEs in residential communities. This data can be used to further understand flood risks and damage at the household level.

ACKNOWLEDGMENTS

I would like to thank my committee chair Dr. Highfield for presenting this research opportunity to me as well as Dr. Brody and Dr. Fortenberry for their additional support and guidance throughout my coursework and research.

Funds to purchase equipment for this research provided by the TCRF

Special thanks to Benjamin M. Ritt for support and guidance with this research as well as sharing equipment used to collect information used in this study.

Thank you to my close friends, roommates, colleagues, and department staff and faculty for making my efforts at Texas A&M University at Galveston memorable and heartwarming.

Finally, thank you to my mother, siblings, and family for their motivation, unwavering support, patience, and love.

CONTRIBUTERS AND FUNDING SCOURCES

This research was supervised by a thesis committee consisting of Chair Dr. Wesley Highfield of the Department of Marine Sciences, Co-Chair Dr. Samuel Brody of the Department of Marine Sciences, and Committee Member Dr. Brent Fortenberry of the Department of Architecture.

Funds to purchase equipment used to collect and process data for this research were provided by the TCRF and Center for Texas Beaches and Shores (CTBS). Equipment bought included DJI Phantom 4 RTK (P4RTK), Pelican Air 1615 case with foam, Garmin GPSMAP 64st, and multiple HyperX RAM Memory sticks. Funding was also provided to support a Graduate Assistant Researcher (GAR) position for the student to fulfill work related to this research.

Coastal Resource Manager, Dustin Henry, and Planning Technician, Karen White, with the City of Galveston Planning and Development Division provided Certifications of Occupancy (COs) and Elevation Certificates (ECs) to compare with FFEs obtained using the UAS. CO and EC data is limited due to voluntary participation in the National Flood Insurance Policy (NFIP). 70 ECs were cross-referenced with housing units located in the communities used for this research.

Benjamin M. Ritt contributed in sharing another Phantom 4 RTK unit, rod, and remote controller (RC), to link with owned Phantom 4 RTK unit, rod, and RC, ultimately to established known positions and ground control positions (GCPs). Known elevational benchmarks provided by either the National Ocean and Atmospheric Administration (NOAA) or various other private companies and organizations, were not available in certain residential communities.

NOMENCLATURE

AI	Artificial Intelligence
BFE	Base Flood Elevation
CoG	City of Galveston
DEM	Digital Elevation Model
DJI	Dà-Jiāng Innovations Science and Technology Co., Ltd
DPC	Dense Point Cloud
FAA	Federal Aviation Administration
FEMA	Federal Emergency Management Agency
FFE	First Floor Elevation
FIRM	Flood Insurance Rate Map
GCP	Ground Control Point
GHA	Greater Houston Area
GIS	Geographic Information System
GoM	Gulf of Mexico
GPS	Global Positioning System
IMU	Inertial Measurement Unit
LiDAR	Light Detection and Ranging
NFIP	National Flood Insurance Policy

NOAA	National Oceanographic and Atmospheric Administration
PPK	Post-processed kinematics
P4RTK	Phantom 4 RTK Drone
RTK	Real-time kinematics
SfM	Structure from Motion
TST	Total Station Theodolite
UAS	Unmanned Aircraft System

TABLE OF CONTENTS

LIST OF FIGURES

Page

LIST OF TABLES

Page

1. INTRODUCTION AND PREVIOUS LITERATURE

1.1 Introduction

Coastal margins are experiencing increased economic and environmental loss due to various anthropogenic and global changes (Barnes, Morgan, & Roberge, 2001; Nicholls and Lowe, 2004; Islam et al., 2009; Knight and Davis, 2009; Gersonius et al., 2013; Gargiulo, Battarra, & Tremiterra, 2020). Urban sprawl, increasing population, and climate change (i.e. sea level rise, storm intensification) have resulted in higher flood risks and damages as well as negatively impacted surrounding natural systems. Coastal and spatial planners rely on spatial and elevational datasets across multiple scales to fulfill geomatic practices (mapping, GIS), scenario planning, and mitigation and adaption strategies (Barnes, Morgan, & Roberge, 2001; Nicholls and Lowe, 2004; Gersonius et al., 2013; Gargiulo, Battarra, & Tremiterra, 2020). Available large-scale datasets make accurate measurements and damage assessments at smaller scales difficult, thus providing decision makers with data gaps for vulnerable communities and high-interest areas. Gathering data at smaller scales can be costly depending on the extent of the area, resolution, and equipment used. The use of an airplane for aerial scanning or imagery could cost upward of 20k USD. To address the lack of alternatives for a cost effective, efficient measurement tool in gathering spatial and elevational data, this study proposes the use of a drone coupled with photogrammetry methods to capture small scale data. Specifically, using the drone as a tool to capture measurements important in assessing inundation risk and damages.

1.2 UAS technology for PaRS and 3D modeling

Unmanned Aerial Systems (UAS), often referred to as drones, have undoubtedly created a competitive market niche with various applications (Colomina and Molina, 2014; Colomina et

al., 2008, Cho et al., 2013; Mayr, 2013; Petrie, 2013). UAS assist in gaining missing information or monitoring on-going functions such as Non-Military Governmental (civil security), emergency response services (forest fire spotting), energy and communication networks (pipeline monitoring), agriculture and fisheries (crop and population monitoring), engineering practices (structure integrity), cultural heritage (archeological site reconstruction), and general intelligence, surveillance and reconnaissance. Regardless of the UAS type, fixed winged or multirotor, these systems have evolved with technology gaining new functions geared towards geomatic applications such as photogrammetry and remote sensing (PaRS) and 3D modeling (Eisenbeiss, 2009, Rakha and Gorodetsky, 2018). These complex UAS systems are built upon subsystems (i.e., internal and external sensors, inertial measurement units (IMUs), autopilot and navigation systems, camera compatibility software, payload sensing, image orientation and camera calibration). This complexity is required though as the applications for the use of the UAS for PaRS and 3D modeling must be accurate.

Photogrammetry and remote sensing involve the use of various photographic and scanning methods to further understand the geospatial and topographic characteristics of an area (Eisenbeiss, 2009, Westoby et al., 2012). There are two types of remote sensing active and passive. Active range-based remote sensing involves the use of a transmitted light or energy source which interacts with a medium and is then reflected to and captured by a sensor, such as Light Detection and Ranging (LiDAR). Passive remote sensing involves taking imagery that captures natural light, such as satellite imagery and Structure-from-Motion (SfM) imagery. SfM imagery are overlapping, offset images of an area or 3D structure. These images can then be used for photogrammetry, which uses the captured 2D images to create 3D models using complex algorithms and calculations. While UAS technologies can perform both remote sensing

techniques, previous studies have shown passive SfM methods are cost and labor friendly relative to active remote sensing techniques while still producing high quality dense point clouds (DPCs) and 3D models (Cook, 2017; Westoby et al., 2012). Essentially, if efficiency of operating the UAS for passive SfM imagery is maximized, similar results would occur compared to a costlier active sensing (LiDAR) UAS.

Accuracy of the resulted DCPs and 3D models can vary based on flight parameters, equipment, and region of interest (ROI)(Colomina and Molina 2014; Grenzdörffer, Niemeyer, and Naumann, 2015; Rakha and Gorodetsky, 2018). Traditional methods using real time kinetics (RTK) enabled Global Positioning Systems (GPS) and ground control points (GCPs) allow 3D models to come within +/- 2.5 cm horizontal and +/- 5 cm vertical accuracies. However, to reach these accuracies, up to 40 GCPs must be established (Ritt, 2018; Peppa, Hall, & Mills, 2019). These data requirements call for increased time and labor in the field during deployment as well as after during postprocessing within photogrammetry software, such as Agisoft Photoscan Pro and Pix4D. Many of these digital elevation models (DEMs) are also environmental and low-relief (2.5D), suggesting higher relief areas (built environment) would require even more GCP management and post-processing. Built environment and structural recreation can be modeled using UAS technology as seen with historical monuments and archeological sites (Grenzdörffer, Niemeyer, & Naumann, 2015; Wang and Li, 2007; Irschara et al., 2010). Accurate 3D DPC and models were created by combining methods of UAS SfM capture and terrestrial laser scanning (TLS) to establish 117 GCPs for just one structure.

The tradeoff for saving time and labor involves using active LiDAR equipped technologies. Many of these UAS products costing more than 8k USD not including the RTK equipment or processing software. Total costs for a low tier LiDAR product package could easily

surpass $15k USD. In October 2018, Dà-Jiāng Innovations Science and Technology Co., Ltd (DJI) released an RTK enabled UAS known as the Phantom 4 RTK (P4RTK) costing less than $8k USD. This technology now allows surveyors and fields of application to create georeferenced 3D models without establishing as many GCPs as well as saving post-processing efforts. A study comparing the P4RTK and the Phantom 4 Pro (P4P), showed that camera improvements and RTK enabled networking can achieve planimetric and vertical absolute accuracies of 14 mm and 29 mm (Peppa, Hall, & Mills, 2019). This is achieved through nadir and oblique image capture greater than standard 60% forward and 40% lateral (side) overlaps as well as establishing a few GCPs in the corners of the ROI. This study aims to test the use of the P4RTK for 3D modeling highly dense built environments such as residential communities. I address the research question: can the P4RTK coupled with photogrammetry methods capture indicators of first floor elevations (FFEs) accurate to traditional survey FFE methods used for flood insurance premiums?

1.2 First Floor Elevations (FFEs) and The National Flood Insurance Policy (NFIP)

The Federal Emergency Management Agency (FEMA) recognizes the lowest floor as the lowest enclosed area (including basement)(FEMA, 2020). An unfinished or flood resistant enclosure, usable solely for parking of vehicles, building access or storage in an area other than a basement area is not considered a building's lowest floor; that such enclosure is not built so as to render the structure in violation of the applicable non-elevation design requirements of Sec. 60.3 (FEMA, 2020). Communities are required to obtain the elevation of the lowest floor (including basement) of all new and substantially improved structures. All new and substantially improved structures must have the lowest floor elevated to or above the Base Flood Elevation (BFE). Non-residential buildings may be floodproofed below the BFE. The BFE is shown on the Flood

Insurance Rate Map (FIRM) for zones AE, AH, A1–A30, AR, AR/A, AR/AE, AR/A1– A30, AR/AH, AR/AO, V1–V30 and VE, used to established flood insurance premiums. A-zones are high risk areas subject to water level rise or inundation by the 1-percent-annual-chance flood event. V-zones are described as high-risk coastal areas subject to inundation by the 1-percent-annual-chance flood event with additional hazards associated with storm-induced waves. Both zones result in mandatory flood insurance purchase requirements and floodplain management standards. FEMA based damage curves also recognize that just 1 inch of water above the first-BFE, or floor elevation (FFE), costs on average $26,000 in flood damages (FEMA, 2018).

The National Flood Insurance Program (NFIP) requires participating, or mandatory, communities to obtain and maintain a record of the lowest floor elevations for all new and substantially improved buildings in the regulatory floodplain (FEMA, 2020). The Elevation Certificate (EC) allows the community to comply with this requirement and provides insurers the necessary information for insurance rates in relation to the BFE zones. The ECs contain elevation information including the FFE (C2.a), the second floor if applicable (C2.b), the lowest horizontal member (C2.c), any grade elevation supporting utilities or service to the house (C2.e), the lowest adjacent grade (LAG)(C2.f), and the highest adjacent grade (HAG)(C2.g)(Figure 1).

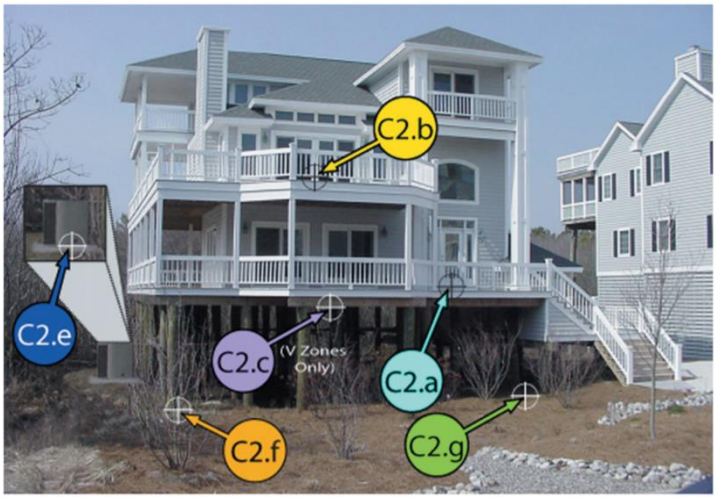

Figure 1: EC information collected shown on a housing unit (FEMA, 2020).

The ECs are obtained through a licensed surveyor, engineer, or architect by using a total station theodolite (TST) and must complete, seal, and submit the EC to the community code official (FEMA, 2020). Robotic total stations (RTS) can cost upward of 10k USD not including labor and other equipment. Not placing the lowest supporting horizontal members and the first floor of a building at the proper elevation in a coastal area can be extremely costly and difficult to correct. Following the carpenter's adage to measure twice, but cut once, the elevation of the building must be checked at several key stages of construction. Note that multiple Elevation Certificates may need to be submitted for the same building: a certificate may be required when the lowest floor level is set (and before additional vertical construction is carried out); a final certificate must be submitted upon completion of all construction prior to issuance of the certificate of occupancy (COs).

1.3 Galveston: City of Storms

Since chartered in 1839, the City of Galveston (CoG) has played a unique role and relation to the history of Texas (City of Galveston, 2020). Galveston was the principal port and gateway to the Southwest during the 19th century. The city furnished shipping, goods, money,

and transportation necessary to settle the state, nurture its trade, and help accomplish Texas independence. Michael Menard bought "one league and a labor of land" in 1836 from the Republic of Texas. He helped organize the Galveston City Company in 1838. From 1840 to 1870, the city was a major immigration port for over a quarter million Europeans (CoG, 2020).

Texas' secession from the Union and the Civil War halted development temporarily, however, the mid-1870s to the mid-1890s was the apex of Galveston's prosperity. The Strand became the “Wall Street” of the Southwest. Fortunes were made in cotton, mercantile house, banks, publishing and printing, flour and grain mills, railroads, land development, and shipping. In 1891, the University of Texas Medical Branch (UTMB) was established (CoG, 2020).

The boom period of the "Queen City of the Gulf" ended with the Great Storm of 1900, a hurricane which killed 6,000 people and left 8,000 homeless. After the storm, the construction of the 16-foot-high, 17-foot-wide seawall was begun (Davis, 1974). The first section spanning from 6th to 39th street was completed in 1904 in addition to 2,200 structures raised an average of five

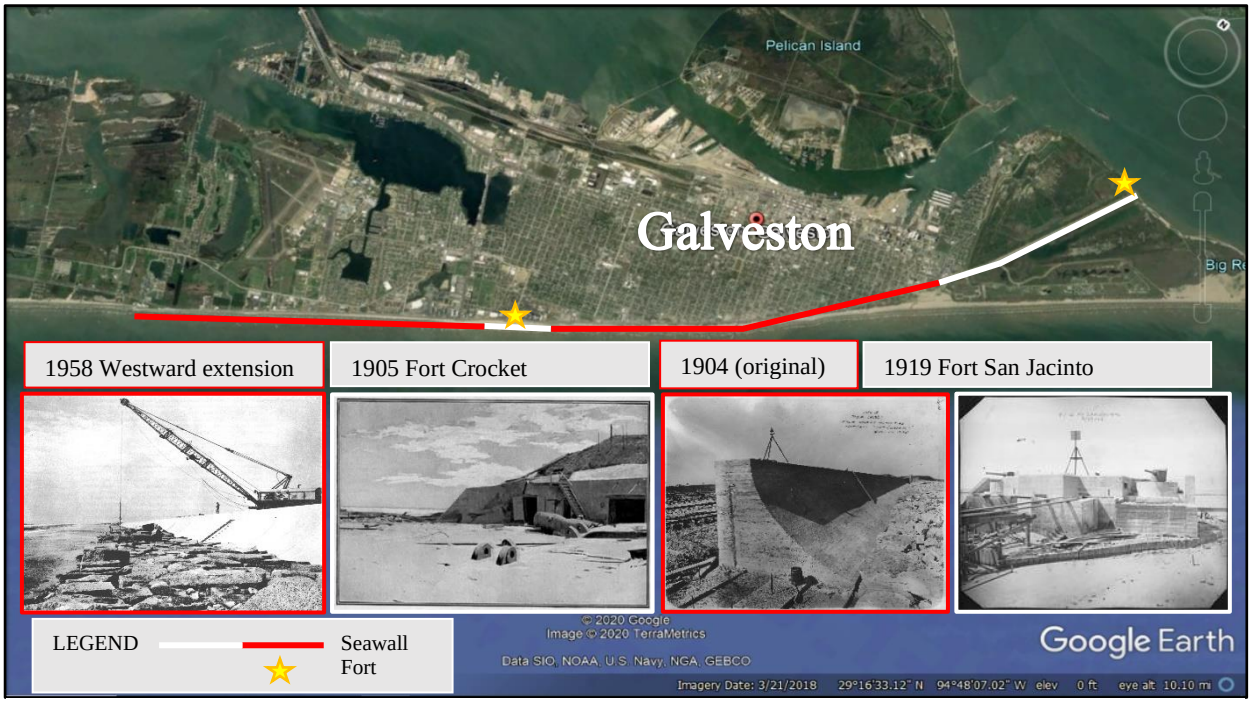

Figure 2: Galveston Seawall extensions by date (created with Google Earth).

feet behind the seawall. Shortly after in 1905, an extension westward to 59th street was approved for Fort Crocket. Fort San Jacinto established on the east end of the island called for an extension eastward in 1919. Multiple extensions westward delayed due to wars and hurricanes were finally completed in 1958 (Figure 2)(Davis, 1974; USACE, 1981).

Texas and Galveston Island have had a large share in hurricanes that have developed in the Atlantic and Gulf of Mexico (GoM)(Roth, 2010). Records dating back to the 1850s indicate that Texas received approximately 120 hurricanes and tropical storms producing an annual probability of 0.8. While intensity of these storms varies by year, data also suggests a major hurricane strikes every 4–5 years. Major hurricanes specific to Galveston landfall include Alicia, Jerry, and Ike. Coastal and inland cities surrounding cities that are directly affected by landfall still experience damages from rainfall and flooding (Islam et al., 2009; Roth, 2010). While the Galveston Seawall protects against certain landfall damages such as wave action and beachfront flooding, the structure does not protect against damages from wind, bayside storm surge, and rainfall flooding. Hurricane and precipitation intensity are expected to increase due to climate trends (i.e., air and ocean warming, sea level rise)(Knight and Davis, 2009; Donat et al., 2016; Pfahl et al., 2017). As a result, studies specific to Galveston and Galveston Bay confirmed that Hurricane Harvey, which made landfall just east of Rockport, caused environmental and housing damages primarily due to rainfall (Du et al., 2019; Du and Park, 2019; Amadeo, 2019).

Galveston today may not be the dynasty it once was; however, the city is still a valuable asset in multiple dimensions. Economically, the Port of Galveston and relations with the Houston ship channel allow for shipping, fishing, and shrimping functions (CoG, 2020). Tourism is also an integral part of the Galveston Island Economy (TE, 2016). In 2016, visitors spent $780 million generating $1.1 billion in business sales and $158 million in tax revenues. Visitor volume and

spending have been increasing on average 2% annually since the 2008 recession. This includes lodging, food, beverages, retail, recreation, transportation, second homes, and cruises form port. Socially, aesthetics of the beach environment and annual events like Mardi Gras and Biker Rally attract visitors to fulfill these economic impacts (TE, 2016). As for second homes, building in high risk areas may not directly affect those who visit rarely; however, socially vulnerable communities within Galveston could experience higher flood risk as a result of homes being built on natural buffers such as the beach and wetlands. Land conversion of natural landscapes to developed impervious alters the overall landscapes capacity to mitigate and store water (Highfield and Brody, 2006; Brody et al., 2007; Brody et al., 2014, Highfield, Brody, & Shephard, 2018).

Since Hurricane Harvey, The United States Army Corps of Engineers (USACE) Galveston District, The Texas General Land Office (GLO), and various other partners, are working to create concept projects that mitigate against future natural disasters and flooding in Galveston and Greater Houston Area (GHA)(USACE, 2020; GLO, 2020). Projects that include beach and bay modifications, multifunctional, or hybrid, structures, and dike and barrier systems. Until then, monitoring vulnerable communities via UAS technology could be valuable in assessing the change created by these projects and their role in reducing flooding or risk.

2. DATA, STUDY AREA, AND APPROACH

2.1 Data

COs and ECs were provided by Coastal Resource Manager, Dustin Henry, and Planning Technician, Karen White, with the City of Galveston Planning and Development Division. The city generally has ECs on file when a home has been newly constructed, or when the property owner is seeking permits to raise the structure out of the flood plain. This is a less common activity and is often seen if the property owner sought a CO from the City. Electronic copies of data available data back to January of 2012.

A dataset of 70 ECs was compiled by cross referencing COs given by the CoG and addresses located in the study areas chosen. The data provided within these PDF ECs along with data collected using the RTK-UAS are the two sources for this study. The following describes the study area where the RTK-UAS methodology will be applied. The instrumentations used to perform measurements, the workflows used to collect and process data, and the elevation certificate datasets that the RTK-UAS measurements will be compared to.

2.2 Study area

Four residential communities located on Galveston Island were chosen as test sites: (1) Lafitte's Cove, (2) Campeche Cove, (3) Evia and (4) Silk Stocking District (Figure 3). Each community contains about 200–300 housing units providing diversity in multiple dimensions. Dimensions including housing structure, location on the island (bayside and central developed), and housing value. Galveston Island offers many diverse residential communities due to the many historical natural disasters that have affected the area. Many houses are abandoned while others are raised or modified to mitigate against future storms. In some cases, previous storm damages made relocation more viable than rebuilding or repairing.

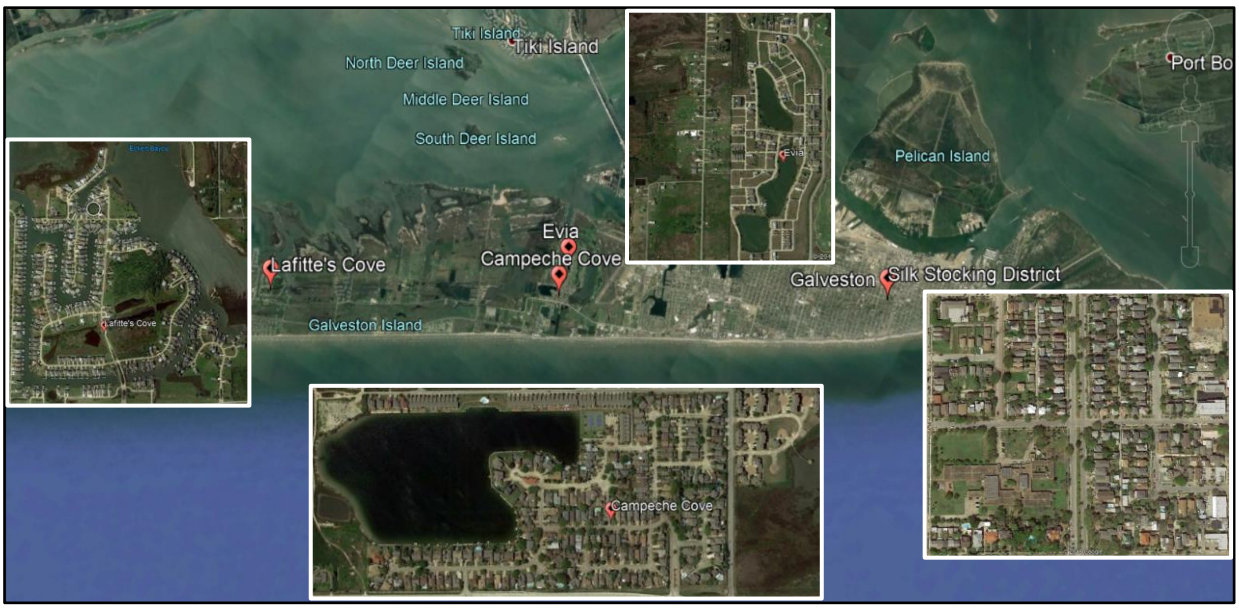

Figure 3: Residential Communities located on Galveston Island: Lafitte's Cove (Left), Campeche Cove (middle, bottom), Evia (middle, top), and Silk-Stocking District (right)(Created in Google Earth, 2020).

2.3 Approach

Given that record of CoG ECs is a function of house modifications through COs or private insurance contracts, FFE data of housing units on the island are limited. This research aims to test if the use of an RTK-UAS coupled with photogrammetric methods is viable in finding indicators of FFEs accurate with traditional EC surveying. Method viability would mean obtaining FFEs would no longer be limited to survey-based ECs under the NFIP. This data can then be used to further understand flood risk, better parameterize flood models and be given to decision makers for planning purposes.

In order to address the lack of alternative measurement methods for obtaining FFEs, estimation of FFEs was sought using an RTK-UAS-based approach. More specifically, a study to address the following research question(s):

1. Can the use of an RTK-UAS and photogrammetry methods find indicators of FFEs accurate to traditional EC methods?
2. Is the use of the RTK-UAS an efficient, cost effective alternative for collecting FFEs at a residential community scale?

The use of the RTK-UAS offers similar, in some cases increased, accuracy compared to previous surveying techniques. Many of the CoG ECs are measured to the nearest tenth of a survey foot. The following hypothesis addresses the comparative analysis of the EC data and RTK-UAS data.

> H_0: FFEs agreement between the CoG ECs and the RTK-UAS data will be high. Whether these datasets are statistically different is uncertain.

This research does not aim to test if the RTK-UAS is accurate. The RTK-UAS accuracy has already been proven. Rather, to test if the use of the UAS-RTK is accurate in capturing indicators of FFEs from external SfM capturing and then using this data for broader planning purposes.

3. METHODS

3.1 Introduction and Deployment Workflow

The P4RTK was purchased in March 2019, 5 months after manufacturer release date. The purchase included the Phantom 4 RTK enabled drone, remote controller (RC), RTK mobile base station, and RTK base station tripod (Figure 4). The RTK enabled drone allows for previous drone surveying functions in addition to high-precision elevation networking. Field deployment workflow was slightly different than other DJI products excluding the RTK base station. Workflow in Pix4D photogrammetry software and field guide used for this research shown in **Appendix A** and **B**.

Figure 4: DJI Phantom 4 RTK (P4RTK).

The workflow and field guide outlines in great detail the pre-flight, field flight, and post flight measures performed for each ROI. This includes the necessary registration, certifications, software updates, and safety precautions related to flying in dense, residential areas. Aside from the physical workflow and field methods, internal mechanical methods related to the drone, camera, and photogrammetry software are tested as well.

3.2 UAS flight parameters testing for 3D modeling at the community scale

As tested in previous studies (Ritt, 2018; Peppa, Hall, & Mills, 2019), drone flight parameters are tested to assess accuracy and quality of 3D models prior to fulfilling overall study. Drone flight parameters effect many other functions and results including flight time, memory/storage, photogrammetry software processing, and 3D point cloud/mesh generation. Drone flight parameters tested using the P4RTK include flight plan type, flight altitude, flight

plan area, flight plan margin, gimble tilt, side and front overlap, oblique side and front overlap, and start and end point of flight mission. Due to the nature of new technology, testing these parameters strived for efficient use of the methodology under certain conditions while still producing quality 3D models.

Flight plan type *– 3D photogrammetry flight plans including double-grid and multi-oriented*

Flight altitude *– altitude(m) at which the drone captures aerial imagery*

Flight plan area *– area of flight plan type based on ROI or sections of ROI*

Flight plan margin *– flight plan boundaries the drone can or cannot exceed from flight plan area*

Gimble tilt *– tilt of the gimble positioning the camera capturing SfM imagery*

Lateral and front overlap *– 2D/Nadir (90-degree gimble tilt) photo capture overlap percentage*

Oblique lateral and front overlap *– 3D (45-60-degree gimble tilt) photo capture overlap percentage*

Start and end points *– where the drone starts and ends relative to the flight plan and launch point*

Flight plan type - Two flight plan types were explored: (1) double-grid and (2) multi-oriented (Figure 5). (1) The double-grid flight plan involved flight transects similar to 'mowing-the-

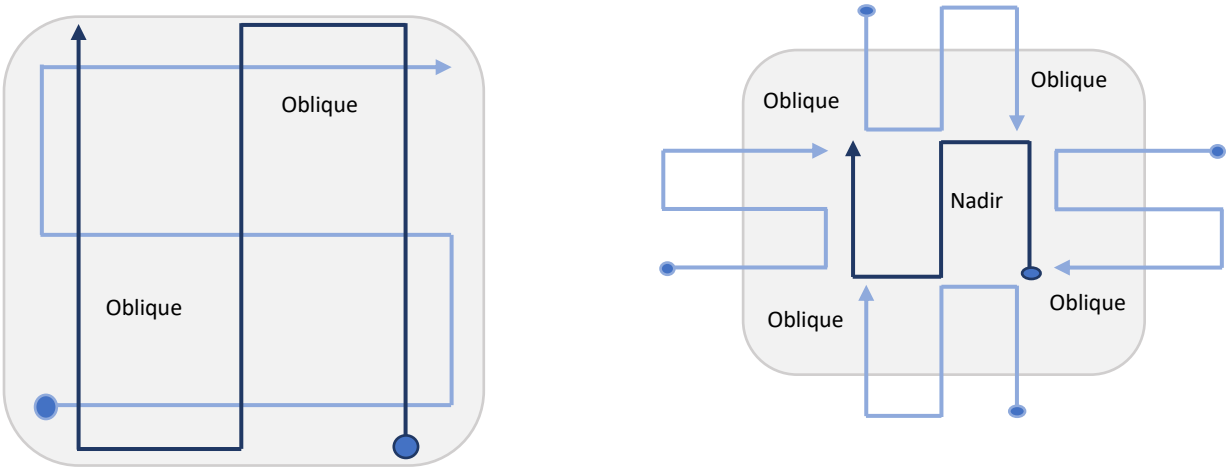

Figure 5: Double grid (left) and Multi-oriented (right). Areas represent ROI.

lawn', or back and forth movements, with two grids perpendicular to each other and oblique gimble tilt. (2) The multi-oriented flight plan involved taking both nadir imagery (90-degree gimble tilt) and oblique imagery of the ROI. It was determined that double-grid worked best in both large and small ROIs areas. In addition to a decreased flight and processing efficiency, the multi-oriented flight plan did not offer improvements in terms of DPC creation. An increase in pictures and flight time required more battery usage and while more pictures could result in a higher quality DPC, the extra images were Nadir, which do not capture oblique angles of built environments. The oblique images captured using double-grid were consistent in capturing the full ROI and providing efficient use of the drone.

Flight altitude - Large ROIs could be flown at a higher altitude (75–100m) while small ROIs could be flown at a lower altitude (45–60m). Lowering altitude would help produce quality 3D models in dense, developed areas (Silk Stocking District) where houses are directly adjacent to each other. Battery efficiency and altitude are correlated; lowering altitude would result in the use of more batteries.

Flight plan area - Flight plan area varies based on the ROI. Depending on battery limitations, ROIs can be divided into subsections and flown at the same parameters. Assigning a large flight area that cannot be completed in a given day due to battery constraints will cause model issues. This is due to the lighting of a particular time or day not exactly matching photos previously shot. The photogrammetry software may have issues with shadows and other differences within a mixed photo population. It was determined that if an area was too large to fly based on time or batteries availability, subsection the area and fly each subsection with exact flight parameters.

Flight plan margin - To increase oblique capture, the margin parameter is set to AUTO. This places the drone flight paths outside the assigned flight area. Switching the margin setting from

AUTO to MANUAL would save battery but reduce oblique capture. In some tests, the outer portions of the Pix4D 3D models were not rendered correctly. This parameter can be customized to fit the unique conditions of a ROI and save about 5–10 minutes of flight time, but not recommended.

***Gimble tilt* –** 60-degree gimble tilt was determined to be the most efficient in capturing oblique SfM imagery. Adjusting between 60-45-degree gimble tilt was in relation to altitude and ROI capture. As gimble tilt was adjusted towards 45-degrees, imagery of the sides of 3D objects were captured at a higher quality, however, so was horizon imagery and objects outside of the ROI (Figure 6). Essentially, at 45-degree gimble tilt, the images captured are exactly half of the ROI and horizon objects. Lowering the altitude while exploring 45-degree gimble tilt works best in capturing as little horizontal, unneeded imagery as possible.

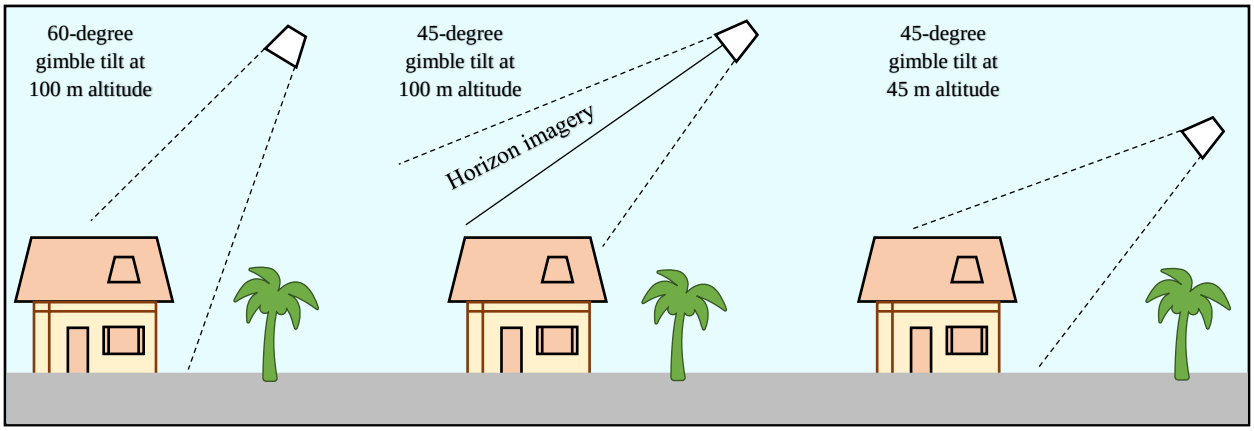

Figure 6: Gimble tilt demonstrations.

Lateral and front overlap / Oblique lateral and front overlap - Because the multi-oriented flight plan type was not used, the lateral and front overlap were parameters were not used, however, tested. The lateral overlap parameter effected battery efficiency and flight time more than any other parameter. Under either nadir or oblique conditions, lateral overlap is defined by the overlap percentage of each photo along each adjacent transect. If lateral overlap was increased, more transects were created within the flight plan thus an increased flight time. Forward overlap

minimally effected battery efficiency and flight time as this parameter increased the percentage overlap of each photo while the drone flew along a single transect. Increasing forward overlap

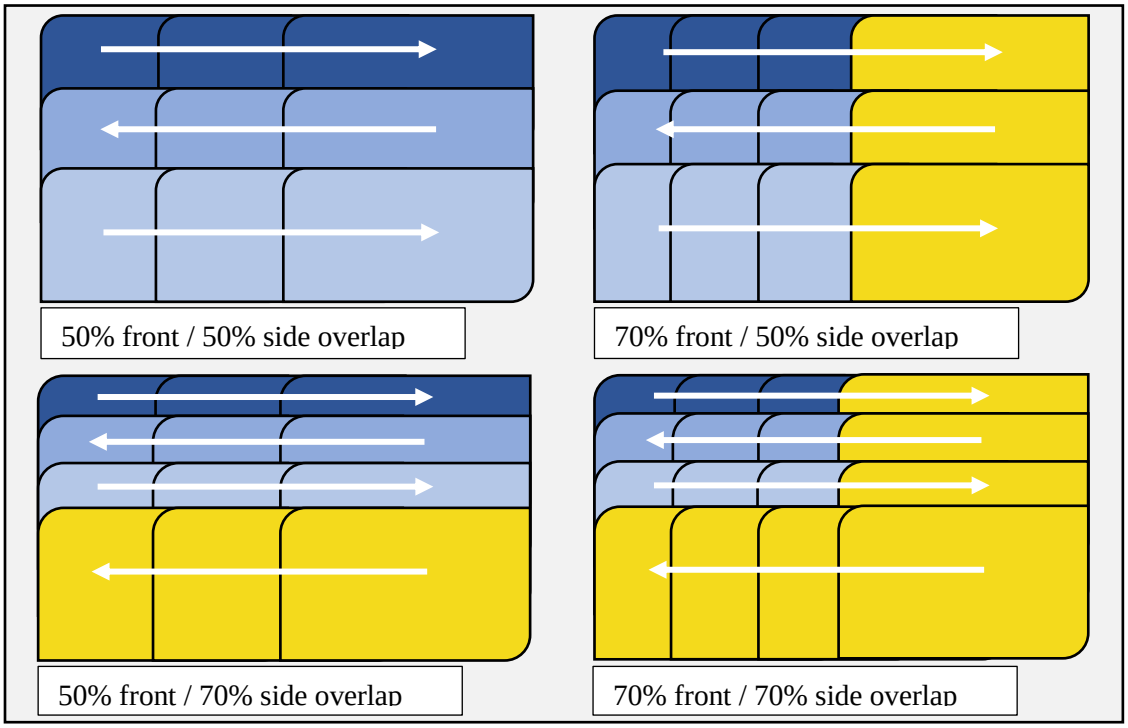

Figure 7: Oblique lateral and front overlap percentage differences. Yellow panels show an increase in transects and photos.

only increased photo count and storage usage and did not create new transects (Figure 7). Automatic settings of 3D flight plan types set both forward and oblique overlaps to 80%. To achieve high quality DPC for 3D modeling, it was determined not to set either of these parameters below 70%, especially side overlap, in exchange to save time or batteries. 3D models and DPCs processed below 70% were inconsistent thus potentially providing inaccurate data. Within a photogrammetry software (Pix4D), less overlap generates less tie points, matched points, and overall points within a DPC and 3D model creating spatial and geomatic discrepancies. This parameter can be adjusted based on altitude. The higher the drone, the less overlap required as the lens now captures a lot more of the ROI in one image.

Starting and ending points – This parameter did not directly affect the outcome of data but has the ability to save flight time and battery life. It was determined that, if possible, establishing the

starting and end points closes to where the drone would take off allows for efficient battery use and flight time reduction. If the ROI is large, establish take off position in the most central location as possible. This would allow for connections to remain stable and overall save battery and flight time.

3.3 Flight Parameters for each ROI

As stated in the flight parameters test, flight area varies by ROI. The residential communities chosen (Lafitte's Cove, Campeche Cove, Evia, and Silk-Stocking District) were all different in area, perimeter, and housing unit density. The table below shows the flight parameters of each residential community flown by the P4RTK (Table 1).

Table 1: Flight parameters for each ROI.

Residential Community	***Flight plan type***	***Flight plan altitude (m)***	***Flight plan area***	***Gimble tilt (degrees)***	***Oblique lateral and forward overlap (%/%)***	***Start and end points***	***Batteries Usage***
Laffite's Cove	Double Grid	100	4 sections (~40-50 acres each)	60	70/75	Closest to launch location. Center of full ROI.	8
Campeche Cove	Double Grid	100	1 section (~61 acres)	60	70/80	Closest to launch location. Outside of ROI.	3
Evia	Double Grid	100	2 Sections (~60 & 115 acres)	60	70/80	Closest to launch locations center of each ROI section.	6
Silk-Stocking District	Double Grid	45	4 sections (~10 acres each)	45	80/80	Closest to launch location. Center of full ROI.	8

3.4 Data Storage

Imagery captured by the RTK-UAS after deployment was saved and backed-up to ensure data security. Approximately a terabyte worth of storage was used for data and back-up data. A total of 7,942 photos were captured across the four study areas (Table 2).

Table 2: Photo analysis for each ROI.

Residential Community	*Avg. number of photos per section*	*Total acres*	*Avg. number of photos per acre*	*Flight altitude (m)*	*Total number of photos*
Laffite's Cove	391/section (4 total)	190 acres	8	100	1,564
Campeche Cove	944	61 acres	15	100	944
Evia	1,158/section (2 total)	182 acres	13	100	2,315
Silk-Stocking District	780/section (4 total)	40 acres	78	45	3,119

Note the image count increases based on section separation and flight altitude. The PDF ECs provided by the CoG were saved and stored as well as converted to match the elevational units captured by the RTK-UAS. Using NOAA's vertical datum conversion tool, the CoG EC elevations were converted from NAVD88 (North American Vertical Datum 1988) survey feet to WGS84 (World Geodetic System 1984) meters (NOAA, 2020). Other data stored included DJI RTK geolocation information and Pix4D post processed files.

3.5 Deriving FFEs within Pix4D

Once image capture was completed, the images were inserted into the photogrammetry software Pix4D. The images are then calibrated, aligned, and stitched together to create a 3D model of the ROIs. To ensure accuracy, minimal post processing kinematic (PPK) efforts, such as including a few GCPs and creating **manual tie points** and **rematch and optimize**, were performed. Additionally, 15 ground control points (GCPs) were established in the Evia community for two reasons: (1) to established new known benchmarks not present in the area and (2) to further test the vertical accuracy of the RTK-UAS with increased GCPs in relation to capturing FFEs. This was done by using the **link with hand-held RTK** function which requires two DJI RTK mobile stations. Benjamin M. Ritt allowed the use of another DJI RTK mobile base station to link and capture GCPs using standard RTK survey techniques. Other ROIs contained NOAA geodetic benchmarks which give accurate vertical control and NAVD88 elevations in meters and survey feet.

Once models were optimized, FFEs of each individual housing unit were then manually obtained within the dense point cloud (DPC) and 3D mesh by finding indicators of FFEs. Indicators include doors, patios, utilities, and change in concrete slab to wood. These indicators are especially obvious in coastal communities as they are often required or recommended to be lifted above BFE, or to the FFE (NFIP, 2020). By clicking on a tie point within the DPC of the 3D model, the X, Y, and Z position is given in northings, eastings, and meters using coordinate system WGS84 and RTK network meters above WGS84 Ellipsoid. Data collected included the FFE, the lowest adjacent grade (LAG), and the nearest draining road (NDR). The LAG is defined as the lowest grade connecting to the base of the house or connecting stairs. The NDR is the closest connecting drainage road to the property. The FFE value used tie points at indicators such as doors,

patios, and utilities. The LAG value used tie points at grade located at the bottom of connecting stairs or housing structure. NDR values used tie points located at lowest edge of a drainage road (Figure 8).

Figure 8: Examples of FFE, LAG, and NDR derivation within Pix4D. Red arrow show data collection points.

Figures 9-12 below show 3D models of the residential communities created in Pix4D. Blur is not a function of quality rather zoom-out and render scale. Red targets represent controlled known positions or established GCPs.

Figure 9: Lafitte's Cove DPC and 3D mesh sections merged. Red dots represent GCPs (processed in Pix4D).

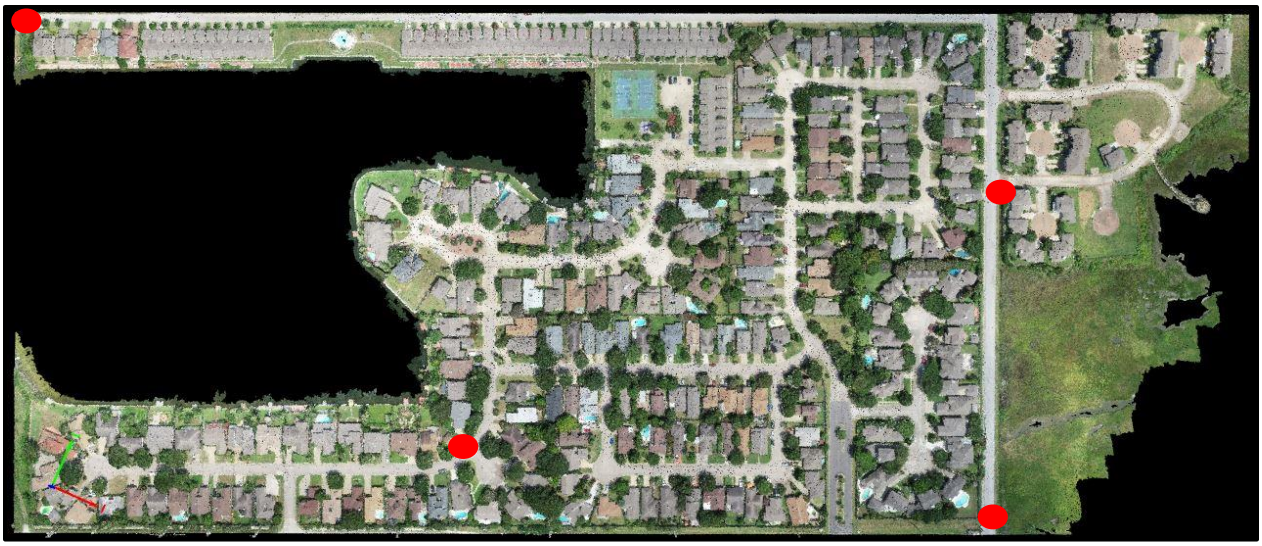

Figure 10: Campeche Cove DPC and 3D mesh. Red dots represent GCPs (processed in Pix4D).

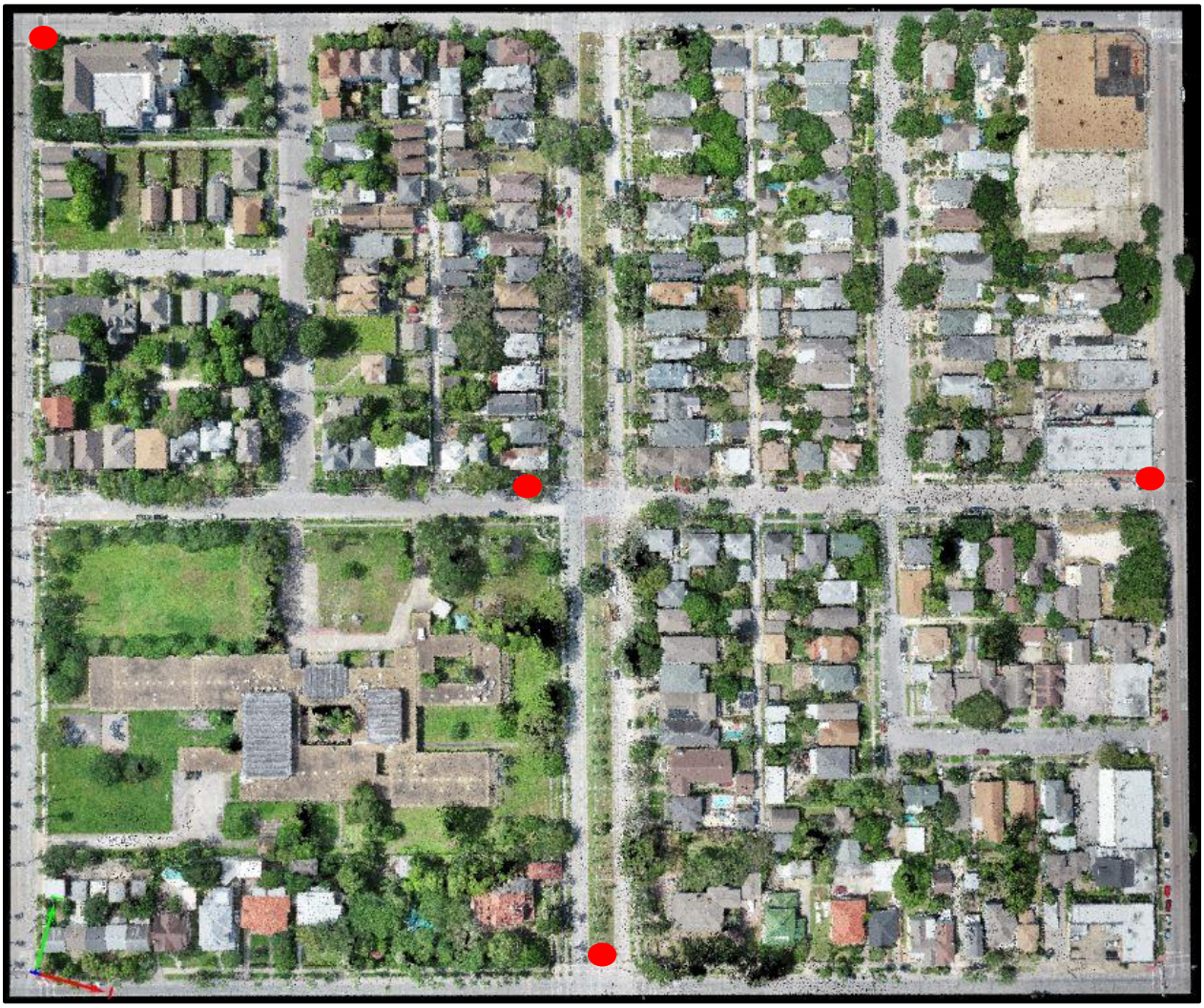

Figure 11: Silk Stocking DPC and 3D mesh. Red dots represent GCPs (processed in Pix4D).

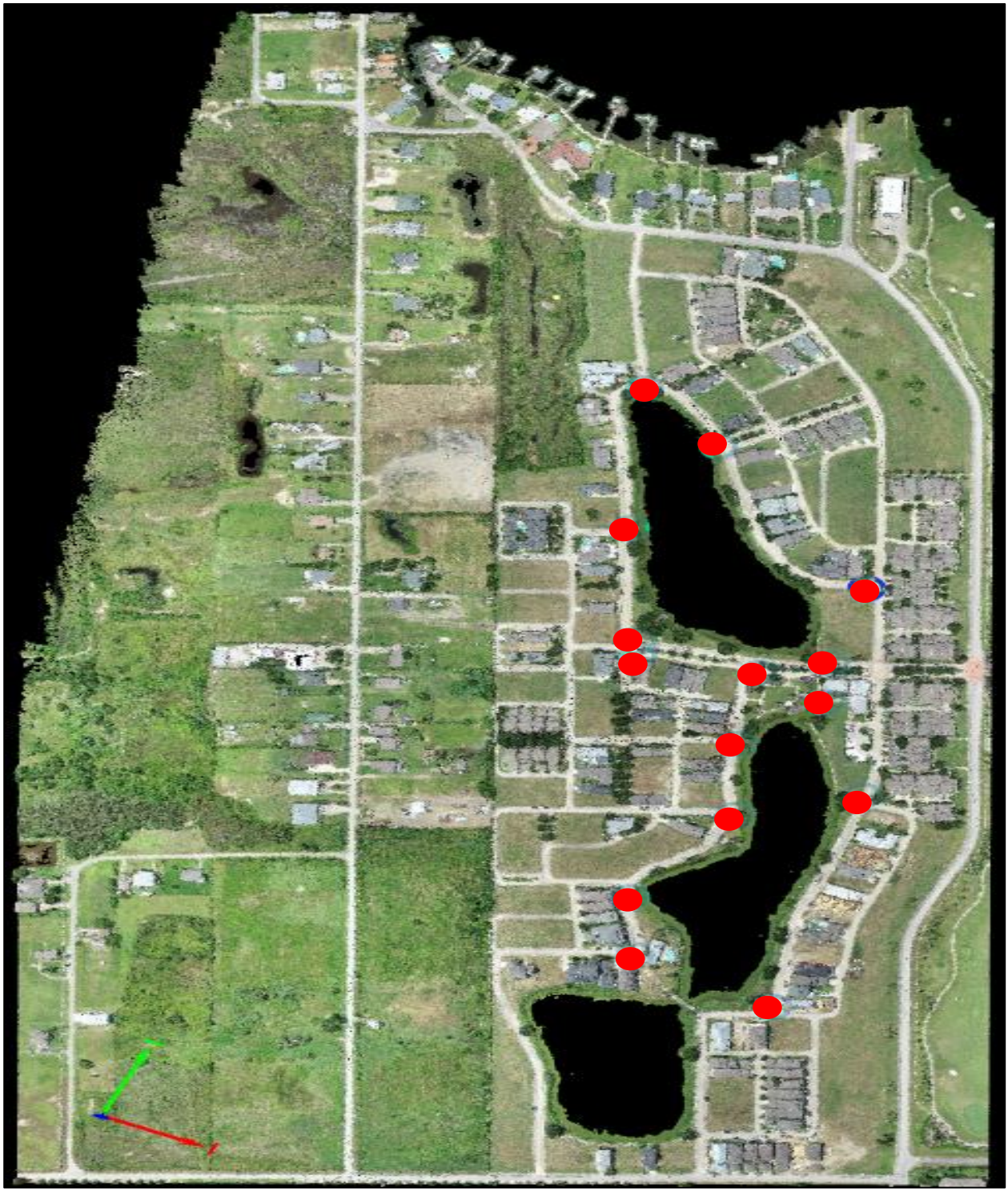

Figure 12: Evia DPC and 3D model. Red dots represent GCPs (processed in Pix4D).

3.6 Comparative Analysis

FFEs within the ECs provided by the CoG and elevations obtained using the RTK-UAS were compared to determine if there was a statistical difference. A paired t-test was performed for the two FFE datasets as well as the LAG elevations. This analysis addressed the research question regarding the role of the RTK-UAS capturing indicators of FFEs accurate to EC measurements. Additionally, a GCP analysis occurred within the Evia community to further confirm the use of GCPs with the RTK-UAS accuracy within densely built environments. Figure 13 shows the full workflow for each ROI.

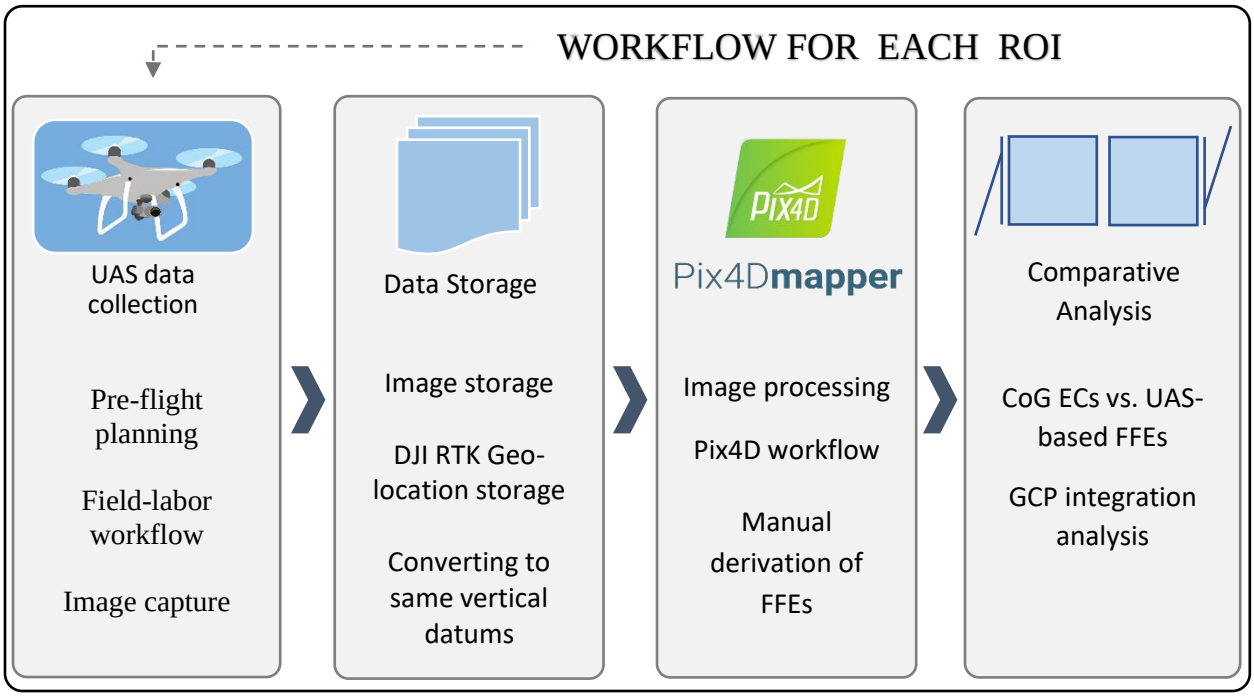

Figure 13: Methods workflow for each ROI.

4. RESULTS

4.1 FFE Comparative Analysis

The use of an RTK-UAS for SfM imagery and photogrammetry produced accurate 3D DPCs and mesh models of the residential communities within Pix4D. Capturing and processing 956 housing units within about a months' time. Manual derivation of the FFEs within Pix4D required additional time, nearly 2–5 minutes per housing unit. Nine ECs were not used from the original 70 provided due to repeated addresses or lack of information, reducing the new population to 61 total ECs. Elevational differences for most (90%) of the housing units were small (<.1 m or 10 cm) while certain outliers (10%) demonstrated inconsistencies with the ECs (Figure 14). Inconsistencies explained after Figure 14 and ECs provided were located in the Evia and Lafitte's Cove communities.

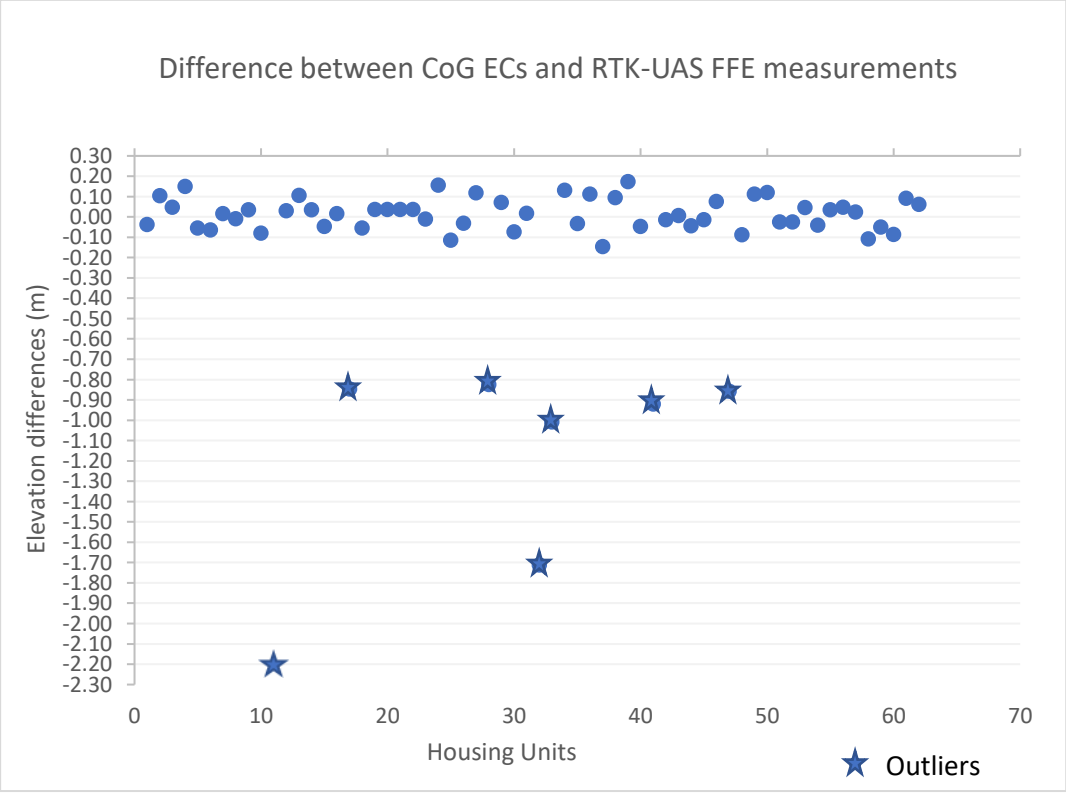

Figure 14: Difference between CoG EC and RTK-UAS FFE measurements.

The FFE difference outliers shown often demonstrate inconsistency with adjacent or surrounding housing unit EC elevations. For example, the first outlier with an elevational difference (ED) of -2.20 m is a housing address that can be compared to similar housing addresses directly adjacent to the unit and with similar housing structure and more accurate FFE difference measurements (Table 3).

Table 3: Elevation difference outlier shown with other similar EC addresses.

Housing Address	**CoG EC elevation (m)**	**RTK-UAS elevations (m)**	**Elevation difference (m)**
4 Duval St	4.42	4.5	.08
5 Duval St	2.16	4.36	2.2
6 Duval St	4.45	4.42	.03
7 Duval St	4.15	4.04	.11

t-Test: Paired Two Sample for Means
With all values

	CoG ECs	*RTK-UAS*
Mean	4.64655	4.75590
Variance	1.08006	0.77389
Observations	61	61
Pearson Correlation	0.90458	
Hypothesized Mean Difference	0	
df	60	
t Stat	-1.91007	
P(T<=t) two-tail	0.06091	
t Critical two-tail	2.00030	

t-Test: Paired Two Sample for Means
Without outliers

	CoG ECs	*RTK-UAS*
Mean	4.85377	4.83685
Variance	0.80997	0.81712
Observations	54	54
Pearson Correlation	0.99652	
Hypothesized Mean Difference	0	
df	53	
t Stat	1.64978	
P(T<=t) two-tail	0.10490	
t Critical two-tail	2.00575	

Figure 15: t-test with all values (left), t-test excluding outliers (right).

The ED outlier shown is similar to the other major outlier with a value of -1.7 m. The CoG EC elevation of this specific address simply does not match the RTK-UAS elevation measurement nor other relative EC elevations and addresses. These outliers could be a function of EC measurement prior to construction and it important to note that these communities are newly built and under constant construction and modification. Other outliers seemed to show the CoG EC elevation measurement closest to the RTK-UAS LAG measurements. Usually a difference of .8-1 m from the FFE measurement.

Comparative analysis of CoG and RTK-UAS FFE were not statistically different in both tests of including all values and excluding the outliers (Figure 15). Although this speaks for the general accuracy of the RTK-UAS indicator approach within Lafitte's Cove and Evia it does not support the strive for extreme accuracies in relation to achieving less than 3 cm per household. About half of the elevation differences were less than 5 cm which is within previous accuracy ranges, however, just outside the 3.5 cm accuracy range. This is not a function of the RTK-UAS accuracy, rather other photogrammetric interpolation limitations explained in the discussion. This is further proven in the GCPs optimization within Evia section.

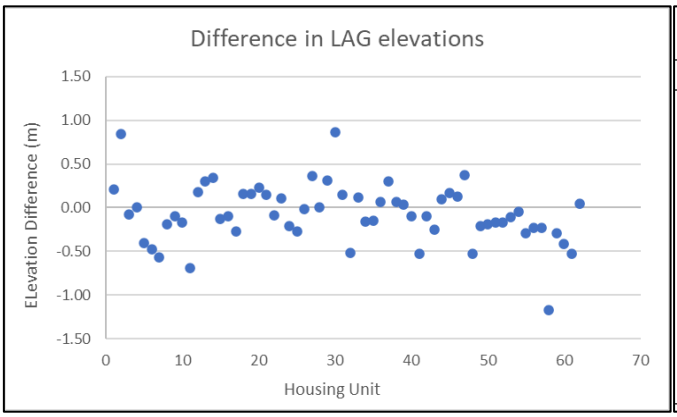

t-Test: Paired Two Sample for Means
All LAG Values

	CoG ECs	*RTK-UAS*
Mean	2.79816	2.87311
Variance	0.55401	0.41501
Observations	61	61
Pearson Correlation	0.89341	
Hypothesized Mean Difference	0	
df	60	
t Stat	-1.74729	
P(T<=t) two-tail	0.08570	
t Critical two-tail	2.00030	

Figure 16: LAG elevation differences (left), t-test paired all values (right).

Comparative analysis of the LAG elevations was also not statistically different but presented a greater spread of differences among individual values. This is a result of the derivation method of the LAG elevation within Pix4D not consistent with in person physical survey methods. Indicators of the LAG also are unique for each individual housing unit making it difficult to determine at the time of development or post development what measurement is considered the LAG elevation.

4.2 GCPs within Evia

The increased use of 15 GCP within the Evia community resulted in a minimal increase in accuracy compared to the use of RTK-UAS with minimal (<5) GCPs. The GCPs were strategically placed evenly throughout the ROI to allow for optimization to occur throughout the entire model. Storm drainage manhole covers were used as GCPs as these were easily seen within the drone imagery and 3D models.

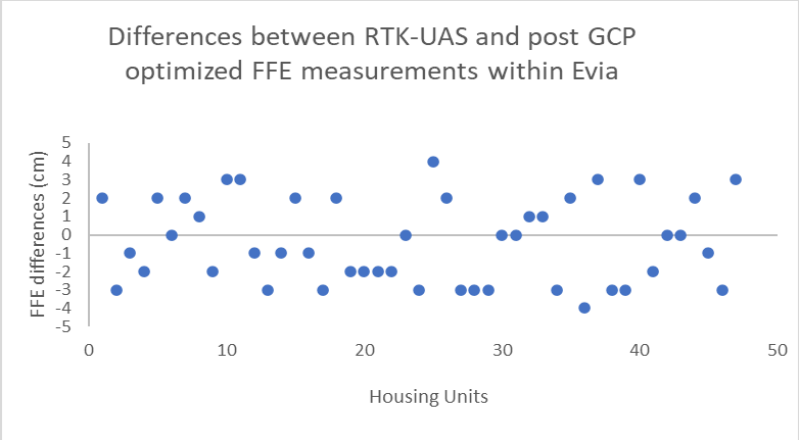

Figure 17: Differences between RTK-UAS and post GCP optimized FFE measurements within Evia.

All measurements optimized by the 15 GCPs within Evia were accurate within 3 cm compared to the RTK-UAS with minimal GCPs which was expected (Figure 17). Increased (>5) GCPs coupled with the RTK-UAS network does provide increased accuracies, however, also

requires another DJI RTK mobile base station to link or other RTK equipment. Additionally, the field labor now requires the creation of a survey plan and capturing the GCPs using traditional surveying techniques. Time and labor are dependent on the quantity of GCPs desired and the area extent of the ROI.

5. DISCUSSION

Overall, this study demonstrates the use of an RTK-UAS for SfM imagery and photogrammetry to ultimately derive FFEs using indicators within densely built, residential communities is viable in achieving measurements accurate to ECs. RTK-UAS technology now presents an alternative method in collecting large amounts of FFE data regardless of flood insurance policy participation in a cost effective, efficient manner. FFE data has broad implications for local, state, and federal planning and management agencies located in flood prone, coastal margins similar to the GHA and Galveston. These areas are subject to increasing change both anthropogenically and environmentally, calling for development modifications due to safety and risk exposures. RTK-UAS technology for FFE derivation in vulnerable, or flood prone, communities can be provided to decision makers at various political and planning levels to reduce impacts from flood events and monitor development changes over time.

RTK-UAS technology in this study was able to capture SfM imagery within four residential communities located in Galveston, Texas in under a month and provide FFE data shortly after. Not only is this method efficient, it also provides a cost-friendly alternative for data collection in high interest economic zones subject to tourism and diverse housing structures. The communities explored in Galveston demonstrated housing structure type, flood zone, and location variability based on EC information and RTK-UAS imagery.

It is important to note that while the RTK-UAS SfM imagery collection is efficient in capturing hundreds of housing units, the FFE derivation process within Pix4D is not automated and must be manually performed. This is not a direct limitation with the methodological approach itself relative to this study, rather a function of time within Pix4D. While this workflow is not automated, it still is a faster method for collecting FFEs compared to individually

surveying each housing unit. Capturing FFEs within Pix4D was done using indicators and elevation values that resemble the FFE or LAG. Given the accuracy of the RTK-UAS is within acceptable scientific and traditionally surveying range, the housing unit indicators captured by the UAS can be used to find FFEs. Indicators such as doors, patios, balconies, and utility structures, are all accepted indicators of the FFE, especially in coastal environments due to housing structures and compliance to NFIP regulations. The ECs capture elevations to the nearest tenth of a foot while the UAS captures elevations within +/- 5 cm. Both similar in measure, however, the UAS approach reduces traditional individual housing unit surveying and allows the capture of entire residential communities. Lack of GCPs or known positions in certain areas were also a limitation, however, was solved by establishing new known points.

The RTK-UAS approach and 3D modeling does have certain limitations with regards to both deployment and data collection compared to traditional survey methods. Firstly, the UAS for SfM capture requires optimal over-head sun lighting, wind conditions less than 25 mph, and zero rain events. These conditions did not present an issue if the necessary preparation and planning was performed, however, battery limitations could present an issue with flight plan extent and mixed photo population. The primary condition that limits the use of the UAS is rain due to the nature of this technology is not waterproof. Wind conditions hardly ever exceeded 20 mph and 3D models can still be generated with moderate cloud coverage, however, not recommended. Secondly, the use of an UAS does require Federal Aviation Administration (FAA) certification and compliance. Meaning the completion of a Part 107 UAS flight test and coordinating with airports if the ROI is within airspace. Certain airspaces have geofencing, which disables drone action within a certain distance. These can be bypassed with the

appropriate approval and verifications. Communication with the air traffic control tower and flight safety precautions were practiced.

Lastly, the UAS SfM allows image capture for static objects. Moving objects, such as water or certain cars, would not render properly and had the potential to interfere with other data points. White surfaces, particularly roofs, had the potential to create too great of reflectance depending on the position of the UAS camera lens in relation to the sun. This would result in points within the DPC elevated higher or inconsistently created. Shadows were recognized as lower relief elevations, or in some cases, resulted in blank points within the DPC. Again, these limitations rarely existed in the densely built, residential community environments if proper planning was performed and rarely affected the ability to derive FFEs.

FFE limitations primarily are a function of the RTK-UAS SfM capture and computing power. The RTK-UAS has the ability to capture accurate aerial imagery, however, the instrument lacks the ability to capture basements if presented. This limitation is considered in other areas that would include basement homes, however, given the coastal extent of the study area, zero homes had FFE basements. Dense vegetation, such as trees and shrubs, occasionally covered a home and was not visible for FFE derivation. Of the 956 housing units, 14 (1.5%) of them were covered by vegetation and unable to derive an FFE. This limitation varies by ROI and can be further explored by changing flight parameters, such as altitude or gimble tilt, however; if the housing unit is completely covered by vegetations, the UAS simply cannot capture the FFE.

The computing power for this study was limited to 32 GB of RAM, an Intel Core i7-6700 @ 3.4 GHz (8 CPU), and an Intel HD Graphics 530 Display graphics card. Specifications listed are low-medium tier for 3D modeling. This limited processing 3D models within Pix4D to MEDIUM instead of HIGH as well as resulted in a longer processing time. Network and cloud

processing workflows can greatly reduce the processing time, however, less customizable and often used for sharing capabilities. With the creation of High-quality models within Pix4D, more points can be generated for the DPC thus mitigating shared values per point. Particularly, horizontal versus vertical point generation. It was observed that horizontal points within the 3D models showed greater exact elevational accuracy compared to a vertical point that shared elevational values. For example, a horizontal pixel that represented a flat patio or door entrance demonstrated an exact elevational value compared to a vertical point along the side of a structure. The vertical points capture a spread of elevational values. This is due to variance within photogrammetric interpolation.

Lack of available data, specifically, EC availability in accordance to residential communities sought in this study was a research limitation. Additionally, the lack of previous studies using this new technology, particularly in dense, built environments, made the methodological approach of this study unique and challenging.

6. CONCLUSION

This thesis explored the role of an RTK-UAS as tool to capture SfM imagery for photogrammetry to derive accurate FFEs in hopes of providing an alternative to traditional EC surveying techniques. After flight protocol testing, flight and photogrammetry workflows, it was determined that the use of RTK-UAS technology can serve greatly in capturing FFE data accurate to previous traditional survey methods. FFE indicators within 3D models of residential communities can be used to capture FFEs as an EC would, however, future work can be done and completely replacing the traditional EC survey process should be further explored. This method is also a cost effective, efficient tool for capturing large datasets of FFEs compared to traditional survey techniques and captures all housing units regardless of flood insurance participation.

Using FFEs manually derived from Pix4D based on RTK-UAS data and ECs provided by the CoG, a comparative analysis was performed showing that there is not a statistically significant difference between the two FFE data sources. While this comparison speaks for the overall accuracy between the two datasets, the accuracy sought for each individual household (+/- 3cm) can be explored further using alternate deriving methods within Pix4D and improved computing power. Future studies should explore the integration of artificial intelligence (AI) as a workflow in Pix4D to automate the derivation process and even possibly increasing accuracy based on indicators. Specifically, photo recognition relative to a certain tie point within a DPC to determine FFE or LAG values.

Preliminary flight protocol testing should be performed for each unique study, however, the one performed in this study provides some guidance with this relatively new technology for future studies that focus on 3D mapping and modeling dense, built environments. Particularly,

environments with potentially less vegetation than a coastal margin, such as inner-city historical or mid-century buildings prone to flooding as a result of impervious surface coverage or other surrounding developmental changes further increasing flood risk.

This work serves coastal and spatial management teams and decision makers with an alternative to monitor and capture FFEs within residential communities subject to high risk flooding from rain events or natural disasters as well as high interest areas that provide environmental or economic benefit. The use of the RTK-UAS captures small scale spatial and elevational data crucial to other practices and mitigation strategies that regional data sets do not accurately assess. This method is also scalable and adaptable across diverse settings creating many implications for flood planning and management. Plans of costly development modifications within coastal margins could seek adoption of this cost-friendly method to assess the mitigation impacts over time, thus allowing resources to be allocated elsewhere in need.

REFERENCES

Barnes, K. B., Morgan, J., & Roberge, M. (2001). Impervious surfaces and the quality of natural and built environments. Baltimore: Department of Geography and Environmental Planning, Towson University.

Cho, G., Hildebrand, A., Claussen, J., Cosyn, P., Morris, S. (2013). Pilotless aerial vehicle systems: size, scale and functions. Coordinates 9, 8–16. https://mycoordinates.org/17004/

Colomina, I. and P. Molina (2014). "Unmanned aerial systems for photogrammetry and remote sensing: A review." Isprs Journal of Photogrammetry and Remote Sensing 92: 79-97. https://doi.org/10.1016/j.isprsjprs.2014.02.013.

Colomina, I., Blázquez, M., Molina, P., Parés, M., Wis, M. (2008). Towards a new paradigm for high-resolution low-cost photogrammetry and remote sensing. ISPRS – Int. Arch. Photogramm. Remote Sens. Spatial Inform. Sci. XXXVII-B1, 1201–1206. https://doi.org/10.5194/isprs-archives-XLII-4-129-2018

Cook, K. L. (2017). "An evaluation of the effectiveness of low-cost UAVs and structure from motion for geomorphic change detection." Geomorphology 278: 195. https://doi.org/10.1007/s00024-017-1730-8

Eisenbeiss, H. (2009). UAV Photogrammetry. Ph.D. Thesis. Institut für Geodesie und Photogrammetrie, ETH-Zürich. Zürich, Switzerland. https://doi.org/10.3929/ethz-a005939264

FEMA, Federal Emergency Management Agency (2020). Information on Flood zones and definitions. Retrieved from https://www.fema.gov/flood-zones.

FEMA, Federal Emergency Management Agency (2020). Information on Base flood elevations BFEs. Retrieved from https://www.fema.gov/media-library-data/20130726-1537-20490 8154/fema499_1_4.pdf

FEMA, Federal Emergency Management Agency (2020). Information on the National Flood Insurance Program and lowest floor. Retrieved from https://www.fema.gov/pdf/nfip/manual201105/content/07_lfg.pdf

FEMA, Federal Emergency Management Agency (2020). Information on the Lowest floor guide. Retrieved from https://images.smartvent.com/images/uploads/codes_and_certs/nfiplowestfloorguide.pdf

Gargiulo, C., Battarra, R., & Tremiterra, M. R. (2020). Coastal areas and climate change: A decision support tool for implementing adaptation measures. Land Use Policy, 91, 104413. DOI: 10.1016/j.landusepol.2019.104413

Gersonius, B., Ashley, R., Pathirana, A., & Zevenbergen, C. (2013). Climate change uncertainty: building flexibility into water and flood risk infrastructure. Climatic Change, 116(2), 411 423. DOI: 10.1007/s10584-012-0494-5

Grenzdörffer, G. J., Niemeyer, F., & Frank, A. (2015). Symbiosis of UAS photogrammetry and TLS for surveying and 3D modeling of cultural heritage monuments-a case study about the cathedral of St. Nicholas in the city of Greifswald. The International Archives of Photogrammetry, Remote Sensing and Spatial Information Sciences, 40(1), 91. DOI: 10.13140/RG.2.1.2167.9444

Irschara, A., Kaufmann, V., Klopschitz, M., Bischof, H., Leberl, F. (2010). Towards fully automatic photogrammetric reconstruction using digital images taken from UAVs. Proc. ISPRS Symposium, 100 Years ISPRS - Advancing Remote Sensing Science.

Mayr, W. (2013). Unmanned aerial systems—for the rest of us. In: 54th Photogrammetric Week. Institut für Photogrammetrie, Universität Stuttgart, pp. 151–163.

Nicholls R.J. and Lowe, J.A. (2004). Benefits of mitigation of climate change for coastal areas, Global Environmental Change, Volume 14, Issue 3,Pages 229-244, ISSN 0959-3780, https://doi.org/10.1016/j.gloenvcha.2004.04.005.

Petrie, G. (2013). Commercial operation of lightweight UAVs for aerial imaging and mapping. GEOInformatics 16, 28–39.

Wang, J., Li, C. (2007). Acquisition of UAV images and the application in 3D city modeling. Int. Symposium on Photoelectronic Detection and Imaging, Proc. SPIE 6623, 66230Z-1-11. doi: 10.1117/12.791426

Westoby, M. J. (2012). "Structure-from-Motion photogrammetry: A low-cost, effective tool for geoscience applications." Geomorphology 179: 300.DOI: 10.1016/j.geomorph.2012.08.021

APPENDIX A

Phantom 4 Pro RTK Setup and Field Guide

Federal Aviation Administration (FAA) Licensing and Registration

1. **Become certified under the FAA Part 107 for Small Unmanned Aircrafts (Drones)**

   FAA Registration for Part 107

   https://faadronezone.faa.gov/#/

2. **Make sure your drone is registered with the FAA**

   FAA Drone Registration

   https://www.faa.gov/uas/getting_started/register_drone/

3. **Ensure the area of interest is not in a restricted airspace. If so, ensure air traffic control is notified and approves your mission.**

   Federal Aviation Administration (FAA) Airspace Restrictions

   https://www.faa.gov/uas/recreational_fliers/where_can_i_fly/airspace_restrictions/

   FAA Airspace Map

   https://tfr.faa.gov/tfr_map_ims/html/index.html

Pre-Flight Preparations

1. **Check the weather**
    a. Wind - speeds of 20 mph or greater are not safe to operate a drone. Wind speeds of 15-20 mph will cause batteries to drain faster and potentially result in distorted pictures.
    b. Rain - the drone, controller, and RTK system are not waterproof. Compartments on all devices are open to atmospheric moisture.

2. **Charge batteries for the drone, RC and RTK system**
    a. The DJI Phantom 4 Pro RTK (P4RTK) use the same lithium ion batteries and previous generations, however, the new remote controller (RC) and RTK system share different, smaller lithium ion batteries.
    b. Battery replacement
        i. Drone - Pinch the two ends of the battery and pull outward, then slide another battery in firmly and listen for two clicks.

        ii. Controller - On the back of the controller, using your thumb slide the grey button located below the battery compartment down. The compartment should automatically open. Next, with one hand hold the grey button on the right side of the compartment down while the other and slides the battery downward. Replace the charged battery in the reverse motion to lock in place.
        iii. RTK System - Slide the battery compartment cover downward. Then remove the battery by pulling outward and place the new one firmly in place by matching the charging groves with the receptors in the battery compartment. Re-attach the compartment cover.

3. Create your flight plan and Update devices if needed

a. Turn on the P4RTK RC - press once followed by a press and hold (same for drone and RTK system). Wi-Fi is required upon controller initial setup. Initial setup includes registration and basic information.

b. NOTE: Become familiar with touch screen icons and functions. Swipe from bottom of screen up to show quick functions. Swipe from top of screen down to access setting, brightness, and volume. This may be useful to re-establish Wi-Fi connection.

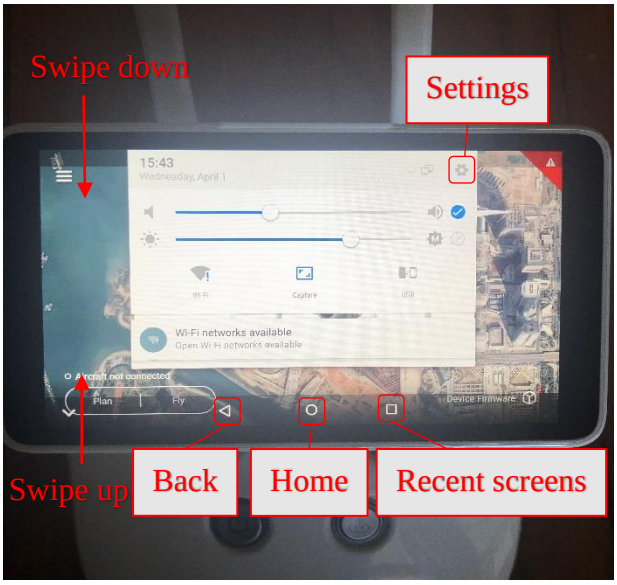

c. In the bottom left corner of the screen select PLAN.

d. Select your flight plan type based on your method approach (i.e., 2D Nadir, 3D).

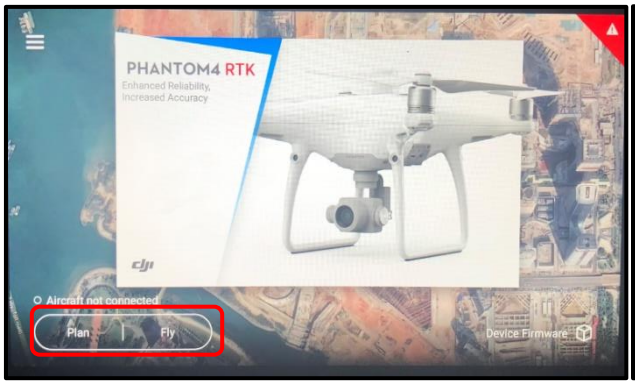

e. Find your area of interest and place at least 3 waypoints to create a flight plan.

f. A small tab with an arrow will appear on the right side of the screen with flight plan settings, camera settings, and advanced settings, that can be adjusted to your liking.

4. **Prepare to take your license and registration cards/paperwork out in the field.**

Field Guide

1. Confirm suitable weather and make sure there are not any high objects that will interfere with flight plan. If applicable, place any ground control points (GCP), scale bars, or site indicators unique to your flight plan.

2. Setup tripod for RTK system at chosen location or over a benchmark. Adjust legs so the level bubbles are centered. There are two level bubbles, one on the tripod and one on the RTK system above the battery compartment.
    a. Insert lower attachment pole of the RTK system and screw in tightly.
    b. Attach upper head of the RTK system and screw in tightly.
    c. Turn on the RTK system by pressing the center power button once followed by a press and hold.
    d. For flights the RTK system must be in MODE 1 which is indicated by the right LED light. Press and hold the MODE button until the LED indicator flashes once to indicate MODE 1. NOTE: To fulfill the Handheld RTK function the second RTK mobile base station must be in mode 3.

3. Turn on the Controller. Angle the two antennas to 45 degrees upward.
    a. In the bottom left corner of the screen, select FLY.
    b. On the left of the new screen, select the document icon. Select PLAN tab and your flight plan.
    c. Next, in the top right corner of the screen select the icon with three dots (Ensure all firmware updates, drone updates, and sensor calibrations are performed).Select the RTK tab and turn on the RTK Function.
    d. Select the RTK Service type and select the mobile station.
    e. If the system does not automatically connect you may select the LINK function at the bottom of RTK Settings and press the link button on the RTK System head. The LED light should flash indicating the attempt to link and turn solid when successfully linked.
    f. This function will then ask to link the aircraft, therefore, having the aircraft on standby, but not turned on, is recommended.

4. Drone Setup
    a. Remove the drone from the case and REMOVE the gimble protector BEFORE turning the drone on.
    b. Attach the color-coded (black and grey) propellers to the correct colored wings.
        i. Black - lock by pressing down and rotating counterclockwise, unlock by pressing down and rotating clockwise.
        ii. Silver - lock by pressing down and rotating clockwise, unlock by pressing down and rotating counterclockwise.
    c. Insert battery and place drone in flat open space. If in a public setting, set up cones or indicators of landing zone.
    d. Turn on drone and have HEX WRENCH provided ready. Select LINK AIRCRAFT on the controller screen and then using the hex wrench press the link button on the drone. The link button hole is located slightly above and between the SD card and connection port.

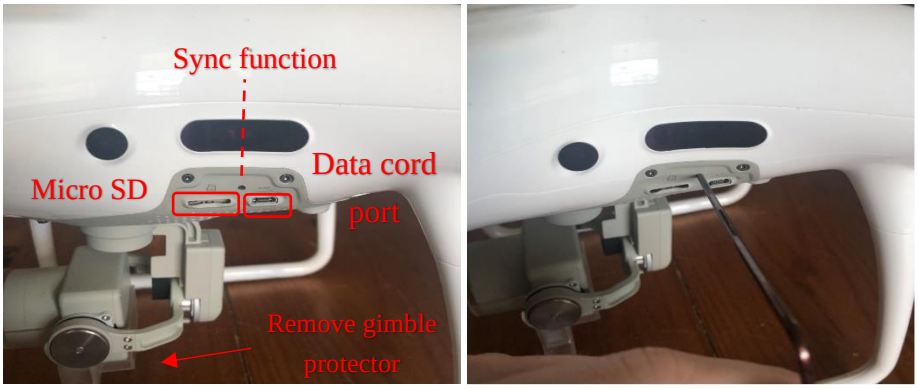

    e. Once linked, all LED lights should turn SOLID GREEN across all devices. If satellite connection is poor, the drone or RTK mobile station may have to be restarted.

5. Executing the flight plan.
    a. If all connections are successful and the drone is ready to take off, select INVOKE located at the bottom right corner of the screen.
    b. Verify checklist and select confirm.
    c. The flight plan will upload and once ready, slide the execute button from left to right.
    d. The drone will begin the flight plan and the battery status are located at the top. If a battery replacement is required mid-flight plan, the return home button can be pressed manually or the drone will automatically return home between 15-20% charge left.

e. To resume the flight mission, DO NOT select PLAN. This function will restart the mission. Select TASK and resume your flight mission. There should be a task completion percentage next to the task. Repeat INVOKE process and resume flight mission.

6. Flight Plan completion and Packing up
    a. Once flight plan is 100% complete and the drone returns home, turn off all equipment and break down the RTK system.
    b. Remove the drone propellers and re-attach the gimble protector.
    c. Place all devices back in case carefully and shut carefully as there may be cords or objects that prevent full closure.
    d. Collect all field objects such as GCP or sale bars, if used
    .

APPENDIX B

Pix4D Workflow

1. Before starting processing within Pix4D, the photos from the micro SD were backed up on another drive and processing saved location was connected to the same folder.

2. Once in Pix4D, **start new project** was selected under the **Project** tab at the top left. NOTE: When merging projects, **Project Merged from Existing Projects** was selected in the same new project window.

3. The project was titled and the location folder was selected where the respective photos were saved.

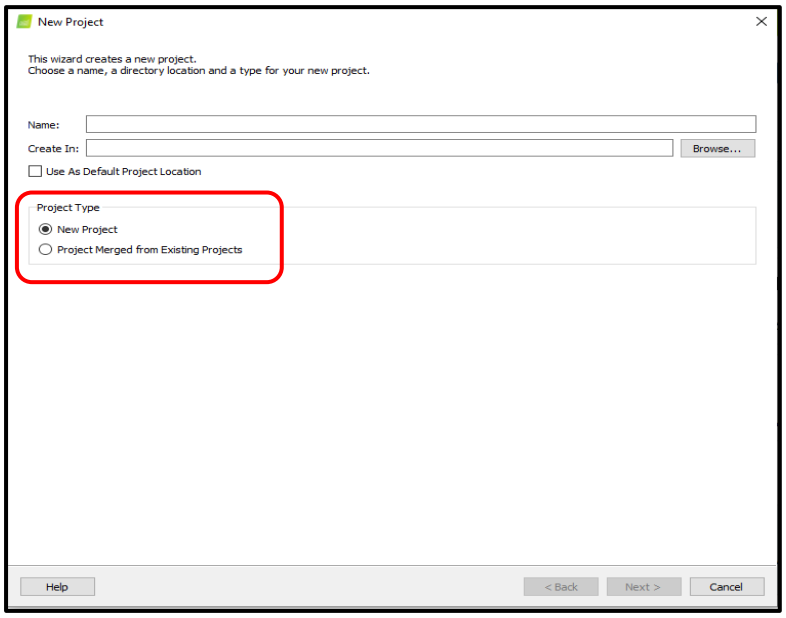

4. Images were uploaded from saved location folder. Ctrl-A was used to select all photos.

5. The images should have geo-information and Pix4D should auto detect the coordinate system and datum. Verify if the two are correct.

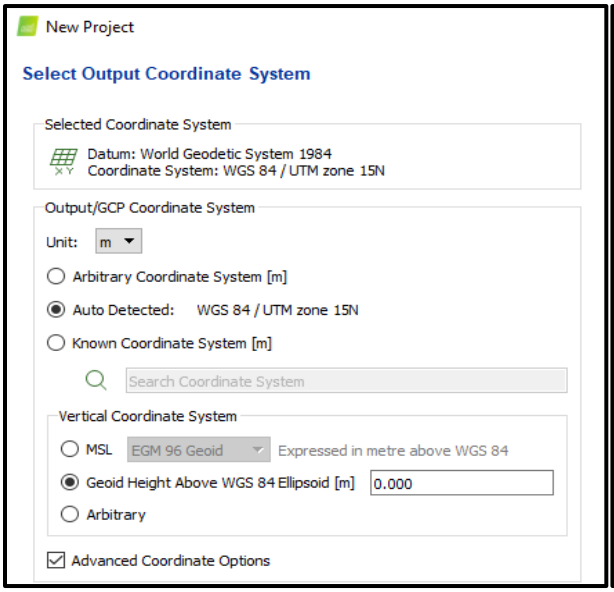

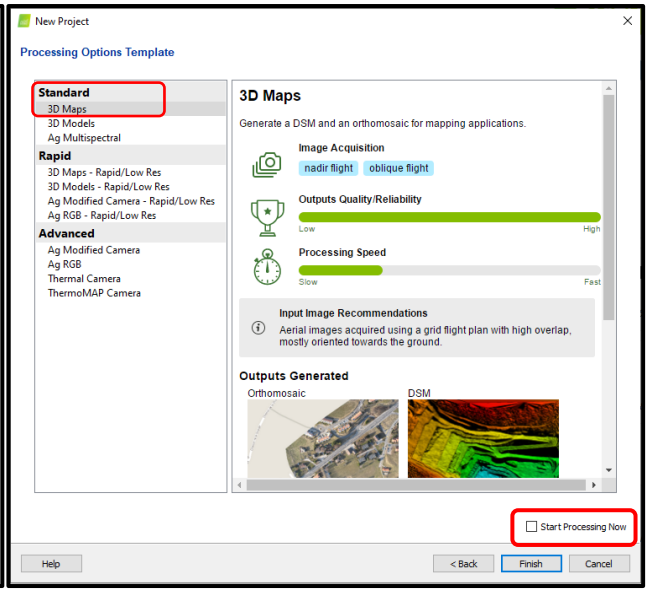

6. Standard 3D maps processing options were selected, not rapid, low quality. **The tiny check box at the bottom which starts the processing was selected to OFF (not checked). Processing was not started at this step.**

7. At the bottom left corner, **Processing Options** was selected to customize and tune calibration settings.

8. Once open, the check box in the bottom left labeled **Advanced** was checked.

9. Then under the processing tab, the **Calibration tab** was selected.

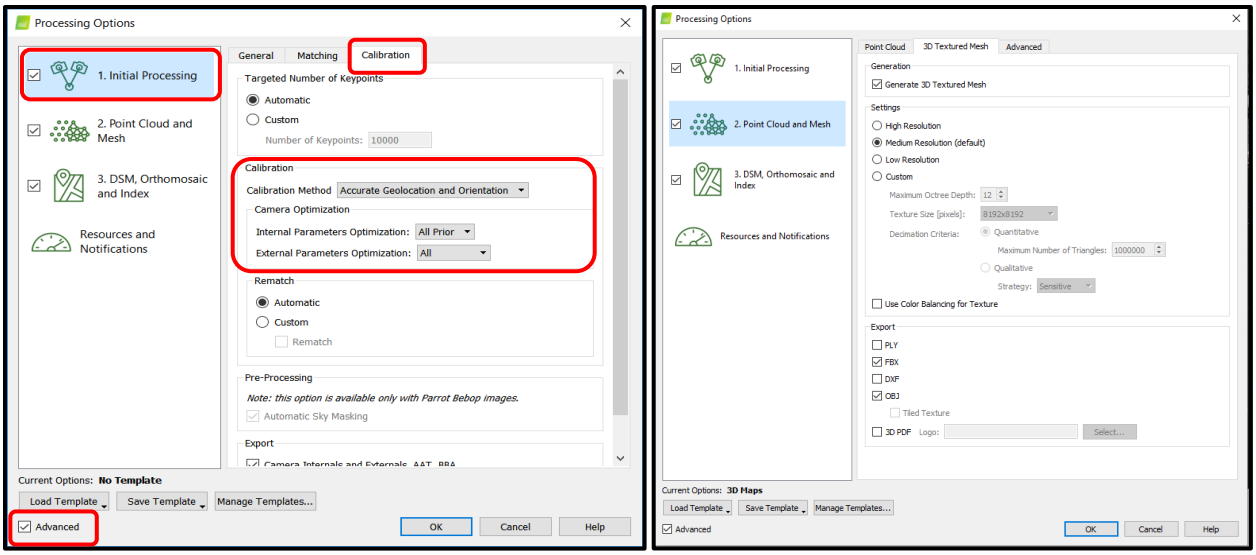

10. Under the **Calibration Method Accurate Geolocation and Orientation** was selected.
    Camera Optimization Parameters were set to the following:
    Internal Parameters Optimization: ALL PRIOR
    External Parameters Optimization: ALL

11. Under the **Point Cloud and Mesh** tab, medium to high quality was selected.

12. **DSM** Settings remained normal.

13. Ground control points (GCPs) were managed and inserted using **GCP/MTP Manager** under the **Project** menu.

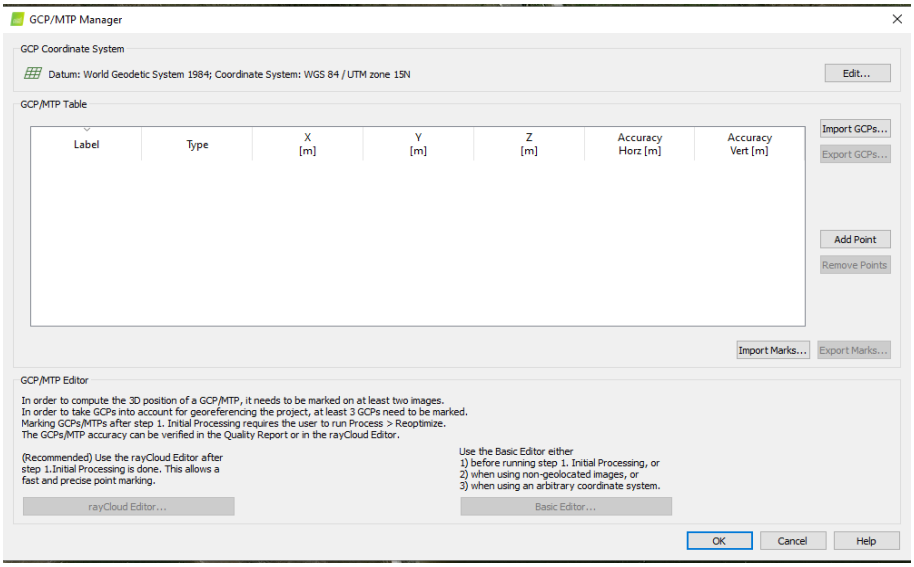

14. **START** was selected to begin processing.